



ELSEVIER

Contents lists available at ScienceDirect

Nuclear Instruments and Methods in Physics Research A

journal homepage: www.elsevier.com/locate/nima

Design and response function of NaI detectors of Aragats complex installation



ARTICLE INFO

Keywords:

Charge-to-code converter
Space weather
Particle detectors
Monte Carlo simulation

ABSTRACT

In 2011, a network of five thallium-doped sodium iodide (NaI(Tl)) detectors was installed on Aragats Space Environmental Center (ASEC) and was included into ASEC detectors system. Along with monitoring of different species of secondary cosmic rays, ASEC detectors register several thunderstorm ground enhancements (TGEs). NaI(Tl) detector integration in the ASEC detector system is of great importance for the study of thunderstorm phenomena for the reason that NaI(Tl) detectors have a higher efficiency of gamma rays detection compared with plastic ones. In this article, the design and characteristics of NaI(Tl) detectors are described. Simulations of detector response are performed. Comparison of simulation results with experimental data showed good agreement between simulations and experimentally observed distributions for analog-to-digital converter (ADC) channels (codes) of NaI(Tl) detectors at two depths of the atmosphere, thus, indicating the correctness of the detector's response determination. A procedure for reconstruction of gamma energy spectrum was developed and approximation of the energy spectrum of recorded TGE event was carried out by a power function under the assumption that the recorded fluxes consist mainly of gamma quanta.

© 2014 Elsevier B.V. All rights reserved.

1. Introduction

The Aragats Space-Environmental Center (ASEC) [1] provides monitoring of different species of secondary cosmic rays and consists of two high altitude research stations on Mt. Aragats in Armenia [2]. Along with solar modulation effects, ASEC detectors register several enhancements associated with thunderstorm activity. The used experimental techniques allowed for the first time the simultaneous measurement of the electrons, muons, gamma rays, and neutrons fluxes correlated with thunderstorm activity [3]. These phenomena are referred to as thunderstorm ground enhancements (TGEs). Ground-based observations with a complex of surface particle detectors, systematically measuring gamma quanta, electrons, muons and neutrons from atmospheric sources are necessary for proving the theory of particle acceleration and multiplication during thunderstorms. Energy spectra and correlations between fluxes of different particles measured on Earth's surface address the important issues of research of the solar modulation effects and the atmospheric high-energy phenomena. Analysis of the resulting energy distributions and correlations between different streams of particles can not only provide information about the atmospheric phenomena and issues related to the effects of solar modulation, but also, provides an opportunity to draw conclusions about the theory of the particles' passage through the atmosphere at high electric fields. These fields are generated by the storm phenomena and lead to increased flows of relativistic electrons, gamma rays and neutrons [4–7]. Detectors located on Mountain Aragats have observed such events repeatedly.

In 2011, a network of 5 detectors with NaI(Tl) scintillators was installed on ASEC [8] to detect low energy gamma rays from the runaway breakdown (RB) process in thunderclouds and particle bursts. Including NaI(Tl) detectors in the ASEC detector system is of great importance for the investigation of thunderstorm

phenomena because NaI(Tl) detectors have high efficiency of gamma rays detection in comparison with plastic ones [9]. Their use allows more precise measurements of the observed fluxes of gamma rays and therefore gives a wealth of information to draw conclusions about the processes of particle acceleration and multiplication by storm phenomena.

2. Design and parameters of the NaI(Tl) detector

Single crystal NaI(Tl) detectors are routine detectors for detecting gamma radiation of low and intermediate energy [9–11]. It has high luminescence efficiency and can be made in a wide range of sizes and shapes. Since the crystal is hygroscopic, it has to be placed in a sealed enclosure. The crystal used had the following parameters: radiation length is $X_0=2.59$ cm, the decay time is approximately $\tau \approx 230$ ns. The wavelength that accords to the maximum of the emission spectrum is $\lambda_{max}=415$ nm, and the light output is equal to 38 photons/keV γ .

Actual detectors consist of $12.5 \times 12.5 \times 30$ cm³ crystal located in a sealed body of 1 mm thick aluminum. A transparent window made of Plexiglass is installed at the end side, and a type FEU-49 Photomultiplier Tube (PMT) is attached to the transparent window. The large photocathode (15 cm in diameter) completely covers the window. The spectral sensitivity range of the PMT cathode is between 300–850 nm, thus, covering the entire spectrum of NaI(Tl) crystal radiation. A schematic view of NaI(Tl) based scintillation detector is shown in Fig. 1.

The block diagram of electronic modules used for detector and data acquisition system is shown in Fig. 2. These electronic modules were developed in the ASEC laboratories for the registration of secondary cosmic rays [12]. They not only replaced the outdated electronics of Nor Amberd and Aragats stations, but also

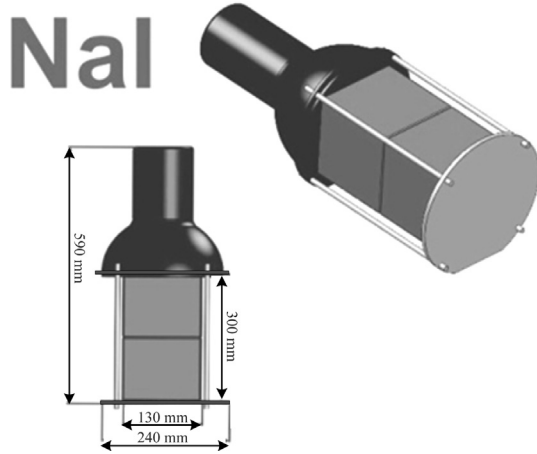


Fig. 1. Schematic view of the detector with NaI(Tl) scintillation crystal.

have fostered the creation of new research facilities for the study of space weather, TGEs, as well as being used in the creation of the global network of detectors [13].

A high voltage transformer, along with the matching buffer amplifier is mounted within an aluminum PMT enclosure, which is a good shield against external noise. The software-adjustable high voltage (HV) converter is used to power the PMT. HV is controlled over the network via an RS-485 interface. Remote control ensures changing the high voltage in the range between ± 900 V and 2100 V with 2 V step. The electronic units of PMT and data acquisition system (DAQ) consume about 100 W and requires a low voltage power supply (DC 12 V) that allows autonomous backup power supply (e.g. solar-powered).

The PMT pulse signal enters the 8-channel pulse analyzer (Fig. 2). The «pulse analyzer» has been created for digitizing the PMT pulses and consistent processing of the data entering its inputs [12]. The input stage of the pulse analyzer consists of an 8-channel logarithmic analog-to-digital converter module (LADC) with programmable threshold, digital-to-analog converters (DAC) to adjust the thresholds, a microcontroller and a serial interface (USB, RS-232, RS-485) for connecting to a computer. The LADC converts the pulse into digital code that determines the number of ADC channel, i. e. the number of bin.

The data collected during one minute are transferred to the PC. Thus, the number of particles and the values of their amplitudes are recorded in codes. Since the LogADC quantization step is about 10.5% of the measured amplitude, the dependence of the amplitude on the code is determined by the following expression:

$$A(K) = A(1) \times 1.105^{(K-1)}, \quad (1)$$

where $A(K)$ is PMT amplitude, which corresponds to the code K , and $A(1)$ is the threshold of LADC corresponding to the least significant bit.

3. Calibration and response function of NaI(Tl) detectors.

Calibration of NaI(Tl) detectors was carried out by comparing the amplitude distribution of the PMT obtained from the fluxes of secondary cosmic rays with the simulation results based on the design features of the detectors.

From calibration experiments on the heights of the mountains [14] it was obtained that 85–90% of the background of charged particles on 1 m² area is that of single particle, the remainder being groups of two or three particles etc. This is the reason why the distribution of energy loss is determined mainly by single charged particles. The fraction of muons and electrons in the high

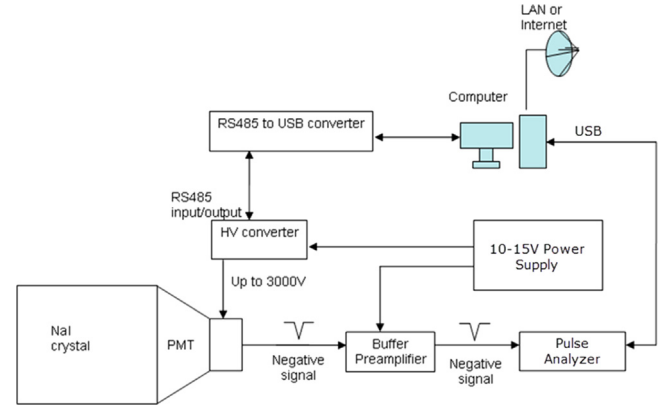


Fig. 2. Block diagram of frontend and data acquisition electronics.

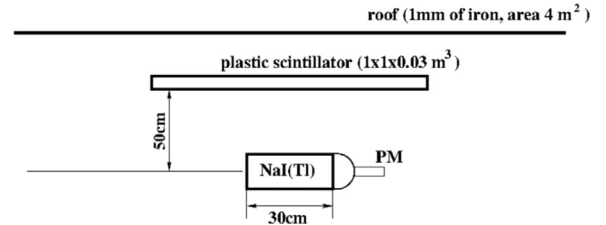


Fig. 3. Schematic of the setup for NaI(Tl) detector testing and calibration.

mountains is approximately $\sim 60\%$ and 30% , respectively, of the flow of charged particles and their ionization losses differ by 5–10% [14–16]. Thus, the observed maximum (mode) K_{MAX} in the distribution of ADC channels is determined by single muons energy losses [14]. Therefore, the detector calibration is reduced to determining the energy deposit in the crystal according to the K_{MAX} . Since the light output of the crystal is proportional to the particle energy loss, then, a similar relation between the energy loss of particles E and ADC channel follows from Eq. (1):

$$E(K) = E(K_{MAX}) \cdot 1.105^{K-K_{MAX}}, \quad (2)$$

where K_{MAX} is the mode of observed distribution of ADC channels.

It is known that the muon minimum ionization losses in the NaI(Tl) crystal are $dE/dX \approx 1.305$ MeV/(g/cm²) [9,17]. The mode of path length distribution in the crystal for incident particles is calculated according to the simulation conditions (angular and lateral distribution) described below and equals to 12.5 cm, which corresponds to $L_{MOD} \approx 46$ g/cm² of matter. Therefore, mode of energy deposit distribution corresponds to $E(K_{MAX}) = E_{MIP} \approx L_{MOD} \cdot 1.305$ MeV ≈ 60 MeV. From Eq. (2), the code K is expressed by E energy losses in the detector as follows:

$$K = \ln(E_K/E_{MIP}) / \ln(1.105) + K_{MAX}. \quad (3)$$

The experimental setup for the investigation of NaI(Tl) detector response is shown schematically in Fig. 3. It consists of 3 cm thick plastic scintillator with an area of 1 m² installed over the NaI(Tl) detector, and 1 mm thick iron roof with an area of 4 m². The design of the plastic scintillator is described in [18,19].

The setup allows observation of the energy deposit spectra of all secondary cosmic rays. Investigation of the neutral component of the secondary cosmic rays is carried out when the signals from the plastic scintillator are used as anti-coincidence (Veto). The operation mode of the NaI(Tl) detector (PMT HV value and discriminator threshold) was established in order to have the peak of the recorded spectrum at channel 31. This ensures that the energy threshold of the NaI(Tl) detector is about 3 MeV, as follows from the Eq. (3).

Simulation of the detector response was performed by GEANT3.21 [20] computer simulation program for the actual layout shown in Fig. 3. We used default mode GHEISHA for hadronic interactions. The simulations were carried out for the flux of secondary cosmic rays (n, p, μ^+ , μ^- , e^+ , e^- , and γ -rays) in the range of energies from 1 MeV to 100 GeV and at two different levels of observation 1000 and 3200 m above sea level, respectively. Fig. 4 shows the differential spectra of the secondary component of cosmic rays obtained by the EXPACS package [21,22], calculated for a location at an altitude of 1000 m above sea level and geographical coordinates 40° 11' North, 44° 31' East.

The fluxes of secondary particles with energies between 1 MeV and 100 GeV have been converted to the number of events in bin. The zenith angular distribution for $\theta < 60^\circ$ is taken in the form of $\cos^{2.5}\theta$ for all types of particles whereas the azimuth angle is uniformly distributed. Figs. 5 and 6 show the detector response simulation results for each component of the secondary cosmic rays along with experimentally observed averaged diurnal data. These results correspond to the above-mentioned two different detector locations, one in Aragats at 3200 m (using a separate detector), and the other in Yerevan Physics Institute at 1000 m using the experimental setup of Fig. 3. The energy deposit of the simulation was recalculated into ADC channels by Eq. (3).

The two peaks are shown in Figs. 5 and 6. The first peak in the region of 5–7 channels is generated by a neutron flux, while the second peak in the region of 31 channel is generated by a muon flux. Neutrons with energies above 1 MeV are detected in the crystal via inelastic scattering. When a muon flux obtained from EXPACS calculations was included in the simulations, the total intensity of spectrum increased in comparison with the experiment. From the shape of the simulated spectrum, it was determined that this increase is due to $\sim 20\%$ muon overestimation. Thus, 20% decrease in the intensity of the muon spectrum led to good agreement between simulated and experimental spectra. The muon fraction in Figs. 5 and 6 is compensated for this overestimation. The agreement between the simulations and the experiment suggests that if $K_{MAX}=31$ and $E(K_{MAX}) \sim 60$ MeV, then, from Eq. (2), the detection threshold of the detector is $E_{TH} \sim 3$ MeV.

Fig. 7 shows the response of the detector to the neutral component of cosmic rays. The experimental spectrum is that of data collected over several hours when the signal from the plastic scintillator is used as anti-coincidence (Veto). Agreement between

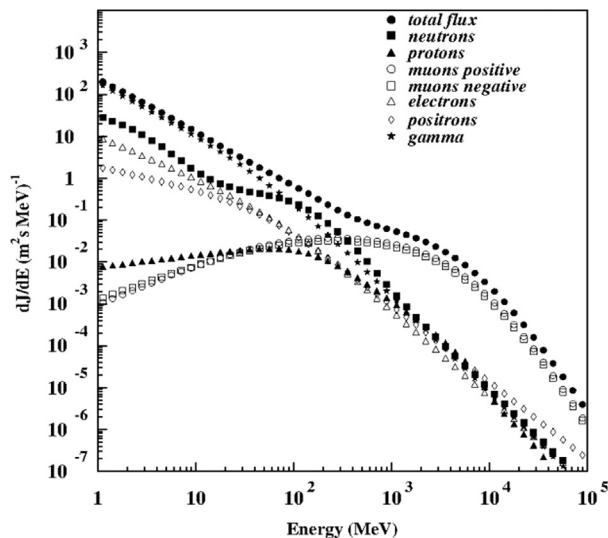


Fig. 4. Simulated differential energy spectra of the secondary cosmic rays components for 1000 m above sea level.

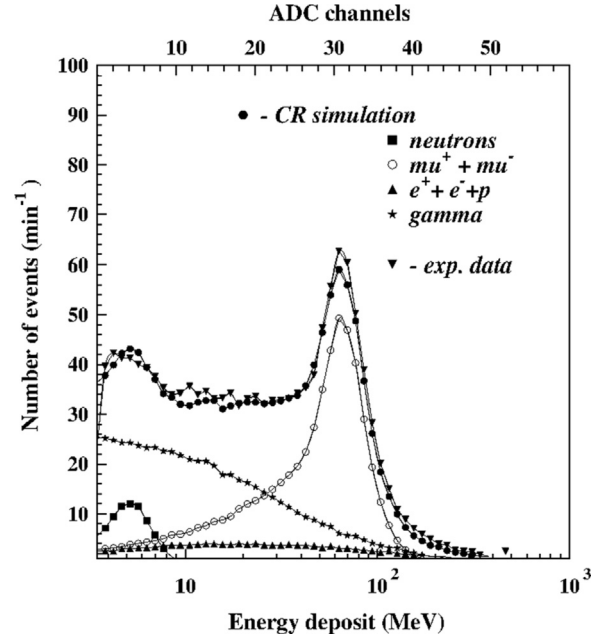


Fig. 5. Distribution of particles by ADC channels and energy deposit. The simulation results and the experimental data at a height of 1000 m above sea level.

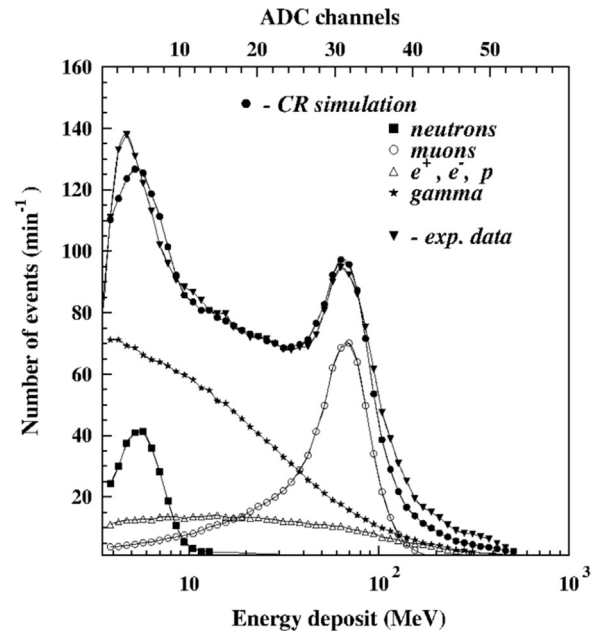


Fig. 6. Distribution of particles by ADC channels and energy deposit. The simulation results and the experimental data at a height of 3200 m above sea level.

the experimental data and the simulations was obtained when 90% detection efficiency of the plastic scintillator for charged particles was included in simulation. The reason for low efficiency was high detection threshold of used detector.

Fig. 8 shows the detection efficiency of the designed NaI(Tl) detectors for the neutral component of the secondary cosmic rays. As shown in the graph, the efficiency of gamma ray detection for NaI(Tl) detector is higher than that of the plastic detectors [8].

A sufficiently thick crystal (at least 5 rad units) allows using the detector as a total absorption detector to measure the energy of particles by their energy loss. The energy deposit E_{dep} in the detector is formed by all the gamma quanta with energies $E_\gamma > E_{dep}$. Some part of the energy $E_{out} = (E_\gamma - E_{dep})$ escapes from registration depending on the location of the gamma-rays interaction point in

the crystal. The relationship between E_{dep} and E_γ has been studied by simulations for the power law spectrum of gamma rays. The simulations were carried out for three values of the power index $\gamma = -1.9, -2.2$ and -2.5 . The simulation for each index contains 5×10^7 hits. The simulation gives an energy dependence on the ADC channel that is uniquely associated with E_{dep} , as can be inferred from Eq. (2). Fig. 9 shows the simulation results of the relationship between gamma quanta energy and the energy deposit in the NaI (TI) detector crystal. As can be seen in Fig. 9, the E_γ/E_{dep} ratio increases with particle energy.

The simulation showed that the power index of the “observed” E_{dep} spectrum agrees within $\pm 2\%$ with primary spectrum embedded in the simulation. Given this fact, the procedure for obtaining spectra E_γ from the experimental values E_{dep} was carried out as follows. The experimental E_{dep} spectrum was approximated by power function. The power index of this approximation was used in simulation to obtain the E_γ/E_{dep} relationship. Then, two-step correction for the reconstruction of the energy spectrum of gamma rays E_γ was performed, i.e. correction for the detection efficiency and for incomplete energy measurement according to obtained E_γ/E_{dep} relationship. Verification with simulated data showed that the proposed technique provides accurate reconstruction of the spectrum intensity in the range of indices between -1.9 and -2.5 no worse than 20%, while for the spectral index the accuracy is within 2%. The intensity accuracy was assessed by

comparing the integral intensity of reconstructed spectrum with total number of simulated events.

4. Gamma quanta energy spectrum of the May 15, 2013 event

Geographically, ASEC is located in a zone of active formation of storm clouds in spring and autumn. The NaI(Tl) detectors are continuously monitoring the fluxes of secondary cosmic rays and increases in the count rate of the detectors have been repeatedly observed during thunderstorms (TGE). One of these events registered on May 15, 2013 is shown in Fig. 10. It can be seen that there is an excess of the count rate of the detectors between 12:20 p.m. and 12:43 p.m. The average count rate at quiet time of all detectors is calculated for the time between 11:00 a.m. and 12:00 p.m. and equals to $1.77 \times 10^4 \text{ min}^{-1}$. In Fig. 11, dotted line shows the average count rate.

According to the ASEC installation data [23], at the peak time between 12:29 p.m. and 12:32 p.m., the event consists primarily ($> 90\%$) of gammas and therefore simulation results are applicable for TGEs analysis.

Fig. 11 shows the energy deposit distribution of CR flux at quiet time (CR), during TGEs (CR+GE) and the energy deposit distribution of excess particles (TGE). The distributions are built for the same timing parameters: CR+TGE for 4 min of event i.e. from 12:29 P.M. to 12:32 P.M., CR average distribution for the quiet time.

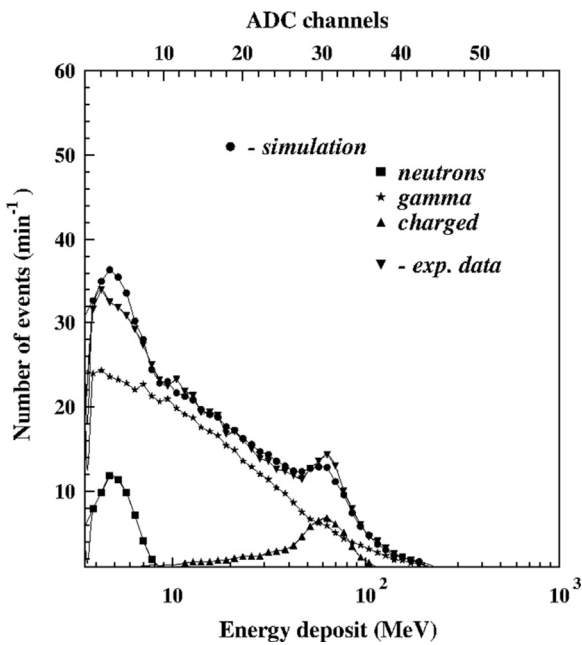


Fig. 7. Simulation results and experimental data for the neutral component at the 1000 m a.s.l. Experimental data obtained when the “VETO” is enabled.

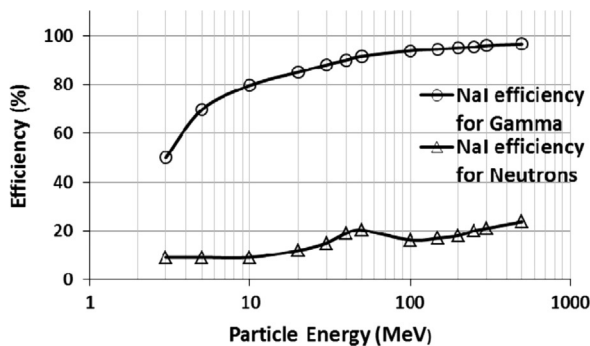


Fig. 8. Detection efficiency of NaI(Tl) detector for neutral components of the CR.

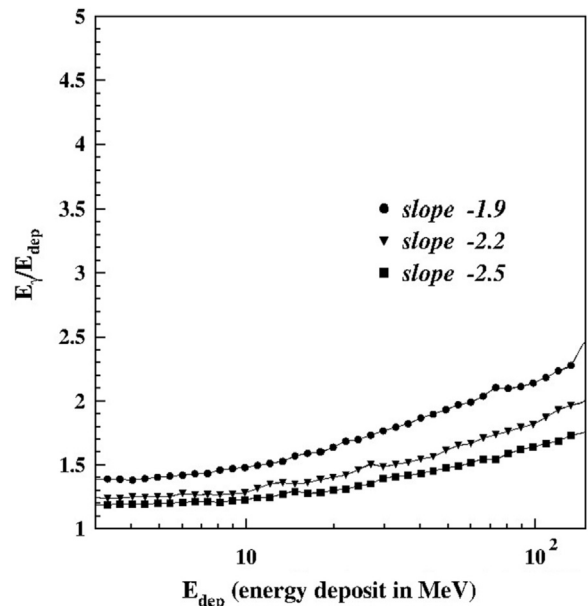
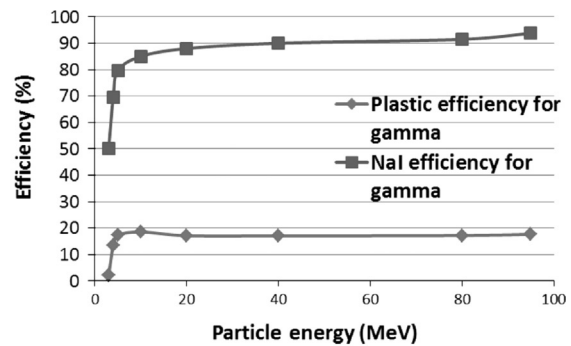


Fig. 9. Relationship between gamma quanta energy and the energy deposit in the NaI (TI) detector crystal.



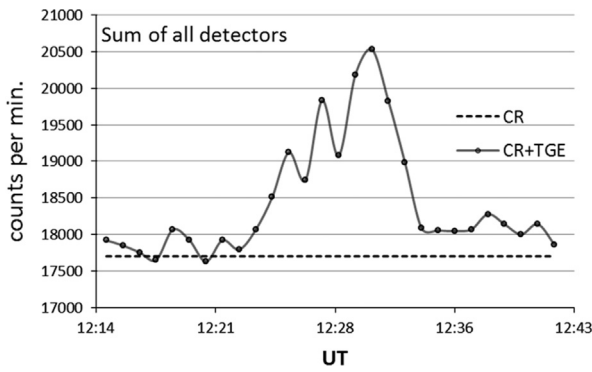


Fig. 10. Timing diagram of the May 15, 2013 event. The dashed line shows CR background count rate at quiet time.

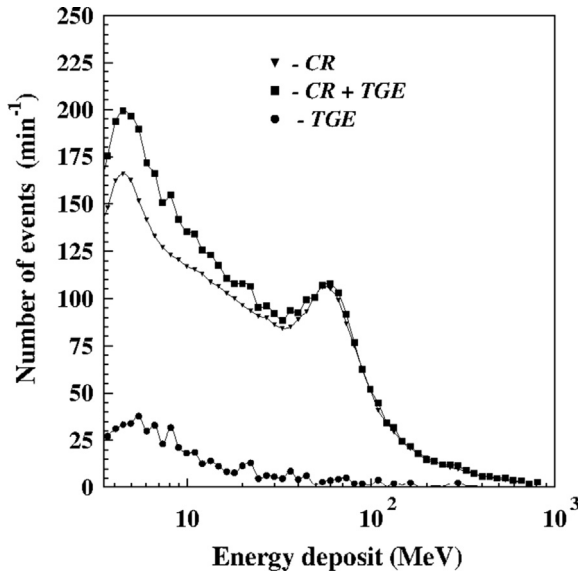


Fig. 11. Energy deposit distribution of CR flux at quiet time (CR), mean value during 4 min of TGE (CR+TGE) and energy deposit distribution of redundant particles in TGE.

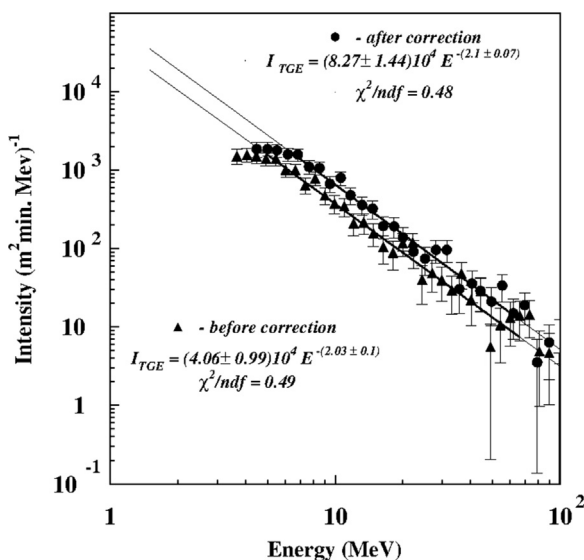


Fig. 12. Corrected (circles) and uncorrected (triangles) energy spectra of TGE's gamma rays.

The average excess of count rate at the specified time is 2167 min^{-1} , which is equal to 12% of the average. At peak time, (12:30) excess has reached 16%.

The first step in the determination of the energy spectrum of excess gamma rays in TGE was performed by Eq. (2). Triangles in Fig. 12 show the distribution of the energy deposit from TGE particles. The distribution was approximated by a power function with an index equal to -2.0 ± 0.1 and intensity $A = (4.06 \pm 0.99) 10^4 \text{ (m}^2 \text{ min MeV)}^{-1}$, ($\chi^2/\text{ndf} = 0.49$). We used the power index -2.0 of this approximation to obtain the E_γ/E_{dep} relationship by simulations.

The spectrum correction of the TGE gamma rays was carried out taking into account the incomplete energy measurement in the detector crystal according to obtained E_γ/E_{dep} relationship. The next correction was carried out taking into account the dependence of detector efficiency given in Fig. 8.

The corrected energy spectrum of gamma was approximated by a power function with an exponent -2.09 ± 0.07 , and intensity $A = 8.0 \pm 1.5 \cdot 10^4 \text{ (m}^2 \text{ min MeV)}^{-1}$, ($\chi^2/\text{ndf} = 0.5$). The spectrum correction leads to a twofold intensity increase, while the slope is the same within experimental error.

5. Summary

A network of NaI(Tl) detectors working on ASEC at Mt. Aragats allows determining the distribution of energy loss of particles in the crystals along with the continuous monitoring of CR. Calibration has been carried out for the purpose of correct reconstruction of particle energy spectra from the values of the ADC channels. Calibration was performed by comparing the simulation results of the cosmic rays passing through the detector with experimentally observed distributions for two depths in the atmosphere i.e. 1000 m and 3200 m above sea level. Comparison of simulations with experimental data showed the following:

- There is good agreement between simulations results and experimentally observed distributions for ADC channels of NaI(Tl) detectors at two depths of the atmosphere, indicating the correctness in the determination of the detector response.
- Eq. (2) allows the correct conversion of the measured ADC channels in the energy deposit in the detector.

The reconstruction of gamma quanta energy has been carried out from the measured energy deposit in the crystal detector. The reconstruction procedure takes into account the incomplete energy measurement in the crystal detector and its dependence on gamma quanta energy. The results showed that spectrum correction leads to a twofold increase in the intensity of gamma rays with energy $E < 100 \text{ MeV}$, while the slope is the same within experimental error.

Approximation of the energy spectra of recorded event (TGE) by a power function was carried out under the assumption that the recorded fluxes consist mainly of gamma quanta.

References

- [1] A.A. Chilingarian, K. Avagyan, V. Babayan, et al., *Journal of Physics G: Nuclear and Particle Physics* 29 (2003) 939–952.
- [2] A. Chilingarian, K. Arakelyan, et al., *Nuclear Instruments and Methods in Physics Research A* 543 (2005) 483–485.
- [3] A. A. Chilingarian et al., in: *Proceedings of the International Symposium on Forecasting of the Radiation and Geomagnetic Storms by Networks of Particle Detectors (FORGES 2008)* [Nor Amberd, Armenia, (Alikanyan Physics Institute, printed by Tigran Mets, Yerevan) 2009], pp. 121–126.
- [4] A. Chilingarian, et al., *Physical Review D* 82 (2010) 043009.
- [5] A. Chilingarian, G. Hovsepyan, A. Hovhanissyan, *Physical Review D* 83 (2011) 062001.

- [6] H. Tsuchiya, T. Enoto, S. Yamada et al. *J. Geophys. Res.* 116, 2011, D09113.
- [7] H. Tsuchiya, T. Enoto, S. Yamada et al. 0708.2947v1 [astro-ph] 22Aug2007.
- [8] K. Avakyan, K. Arakelyan, A. Chilingarian, et al., *Journal of Physics: Conference Series* 409 (2013) 012218.
- [9] C. Grupen, *Particle Detectors*, Cambridge University Press, UK, 1996.
- [10] L.T. Tsankov, A.G. Mitev, CH.B. Lenev, *Nuclear Instruments and Methods A* 533 (2004) 509–515.
- [11] I. Hossian, et al., *Scientific Research and Essays* 7 (1) (2012) 86–89.
- [12] Chilingarian A., Arakelyan K., et al. in: *Proceedings of International Symposium FORGES*, Nor-Amberd, Armenia, 2008, pp. 105–116.
- [13] A. Chilingarian, K. Arakelyan, et al., *Journal of Physics: Conference Series* 409 (1) (2013).
- [14] V.V. Avakyan, et al., *Voprosi Atomnoi Nauki i Tekhniki, Ser. Physical Experiment Technique* 4 (16) (1983) 3–23 (In Russian).
- [15] N.A. Dobrotin, *Cosmic Rays*, USSR Academy Publishing, Moscow, 1963, p. 125.
- [16] Alkofer O.C., Greider P.K.F. *Physics Data, Cosmic Ray on Earth*, 25-1, Karlsruhe, 1984.
- [17] K. Hagiwara, et al., *Phys. Rev. D* 66 (2002) 010001.
- [18] Chubenko AP et al. in: *Proceedings of the 30th International Cosmic Ray Conference*, Merida, 2007, pp. 853–856.
- [19] Ampilogov N.V. et al. in: *Proceedings of the Russian Academy of Science, series Physics*, 71, 2007, p. 580 (in Russian).
- [20] CERN Program Library Long Writeup W5013, (<http://wwwinfo.cern.ch/asd/index.html>).
- [21] T. Sato, K. Niita, *Radiat. Res.* 166 (2006) 544–555.
- [22] T. Sato, H. Yasuda, K. Niita, A. Endo, L. Sihver, *Radiat. Res.* 170 (2008) 244–259.
- [23] A. Chilingarian, G. Hovsepyan, L. Kozliner, *Phys. Rev. D* 88 (2013) 073001.

K. Arakelyan, A. Daryan*, G. Hovsepyan, A. Reimers
Yerevan Physics Institute, AM-375036, Yerevan, Armenia
E-mail address: ara_daryan@mail.yerphi.am (A. Daryan)

L. Kozliner
Yerevan Physics Institute, AM-375036, Yerevan, Armenia
Israel Space Weather Center of Tel Aviv University,
Golan Research Institute and Israel Space Agency, Israel

Received 14 October 2013

5 June 2014

10 June 2014

Available online 19 June 2014

* Corresponding author. Tel.: +374 93 340729.